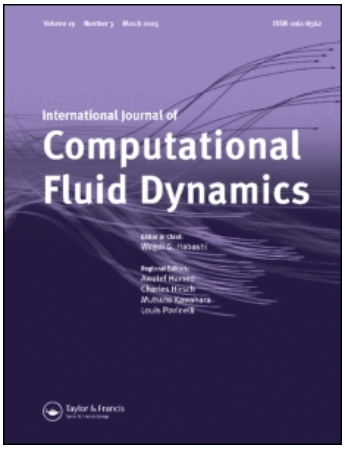

International Journal of Computational Fluid Dynamics
Publication details, including instructions for authors and subscription information:
http://www.informaworld.com/smpp/title~content=t713455064

Simulation of free-surface flows by a finite element interface capturing technique

L. Battaglia[ab]; M. A. Storti[a]; J. D'Elía[a]
[a] Centro Internacional de Métodos Computacionales en Ingeniería (CIMEC) Instituto de Desarrollo Tecnológico para la Industria Química (INTEC), Santa Fe, Argentina [b] Grupo de Investigación en Métodos Numéricos en Ingeniería (GIMNI) Facultad Regional Santa Fe, Universidad Tecnológica Nacional, Santa Fe, Argentina

Online publication date: 09 July 2010

To cite this Article Battaglia, L. , Storti, M. A. and D'Elía, J.(2010) 'Simulation of free-surface flows by a finite element interface capturing technique', International Journal of Computational Fluid Dynamics, 24: 3, 121 — 133
To link to this Article: DOI: 10.1080/10618562.2010.495695
URL: http://dx.doi.org/10.1080/10618562.2010.495695

International Journal of Computational Fluid Dynamics
Vol. 24, Nos. 3–4, March–May 2010, 121–133

Taylor & Francis
Taylor & Francis Group

Simulation of free-surface flows by a finite element interface capturing technique

L. Battaglia[a,b]*, M.A. Storti[a] and J. D'Elía[a]

[a]*Centro Internacional de Métodos Computacionales en Ingeniería (CIMEC) Instituto de Desarrollo Tecnológico para la Industria Química (INTEC), UNL/CONICET, Güemes 3450, Santa Fe, Argentina;* [b]*Grupo de Investigación en Métodos Numéricos en Ingeniería (GIMNI) Facultad Regional Santa Fe, Universidad Tecnológica Nacional, Lavaisse 610, Santa Fe, Argentina*

(*Received 23 October 2009; final version received 5 May 2010*)

Transient free-surface (FS) flows are numerically simulated by a finite element interface capturing method based on a level set approach. The methodology consists of the solution of two-fluid viscous incompressible flows for a single domain, where the liquid phase is identified by the positive values of the level set function, the gaseous phase by negative ones, and the FS by the zero level set. The numerical solution at each time step is performed in three stages: (i) a two-fluid Navier–Stokes stage, (ii) an advection stage for the transport of the level set function and (iii) a bounded reinitialisation with continuous penalisation stage for keeping smoothness of the level set function. The proposed procedure, and particularly the renormalisation stage, is evaluated in three typical two- and three-dimensional problems.

Keywords: transient flows; free-surface; interface capturing; level set method; reinitialisation

1. Introduction

Free-surface (FS) flows are a particular case of multiphase flows, where there is a liquid phase and a gaseous phase, the latter being lighter than the former. Flows with an FS are found in several engineering disciplines, as chemical, mechanical or hydraulic, covering a wide range of fluid properties and flow cases, such as sloshing in liquid storage tanks or open channel flows. In this work, attention is focused on FS incompressible isothermal flows of Newtonian viscous fluids, in the cases where the surface tension is negligible.

There are different approaches for the computation of two-fluid flows, which are described as interface tracking and interface capturing methods (Shyy *et al.* 1996). On one hand, interface tracking methods follow explicitly the FS, which is defined over specific entities, such as nodes or faces of a mesh used with a finite element method (FEM). The domain considers only the fluid phase, and the deformation of the domain, as a consequence of the FS movement, can be solved in different ways. The most common alternatives are Lagrangian approaches, as in particle methods (Idelsohn *et al.* 2004), where fluid particles are free to move, and arbitrary Lagrangian-Eulerian (ALE) approaches (Hughes *et al.* 1981; Huerta and Liu, 1988; Chippada *et al.* 1996; Rabier and Medale, 2003), where the change in the shape of the domain involves either, the deformation of the mesh, keeping the topology constant, or a periodic remeshing, depending on the magnitude of the displacements. In the last alternative, large FS deformations are sometimes hard to model due to the fixed topology, avoiding merging or breaking up of the interface. On the other hand, interface capturing strategies consider fixed tessellations of the two-fluid domain, where the interface crosses a set of elements. The precise position of the FS is captured by an additional quantity, as a scalar field given over the whole domain, or a fluid fraction registered in each element crossed by the FS. Generally speaking, these alternatives allow the folding of the interface without special considerations, although they are not as precise as interface tracking with regard to the FS displacements. The most common interface capturing methods are volume of fluid (VOF) (Hirt and Nichols, 1981; Scardovelli and Zaleski, 1999) and level set (LS) (Osher and Sethian, 1988; Sethian, 1995). The former is based on the definition of a fluid fraction F on each element of the discretisation, being $F = 0$ in the gaseous phase, $F = 1$ in the liquid one and $0 < F < 1$ for cells crossed by the interface, which is recovered by specialised algorithms. On the other hand, LS methods consider an additional scalar variable, the level set function ϕ, which is advected by a transport equation, identifying the liquid phase with positive values ($\phi > 0$), the gaseous phase with negative values ($\phi < 0$) and the interface with null values ($\phi = 0$).

*Corresponding author. Email: lbattaglia@santafe-conicet.gob.ar

ISSN 1061-8562 print/ISSN 1029-0257 online

DOI: 10.1080/10618562.2010.495695
http://www.informaworld.com

In previous works (Battaglia *et al*. 2006, 2007), an FEM-ALE strategy was developed for solving FS fluid flows such as sloshing in tanks. However, the proposal was limited to flow cases where the uniqueness of the interface was verified.

The aim of this work is to apply an LS interface capturing approach for solving two-fluid flows in a single domain, considering both phases as Newtonian, viscous and incompressible fluids. In the present case, each fluid is indicated with a positive or negative value of the LS function ϕ, as described before. The ϕ-field is continuous over the whole domain, including the transition across the FS, given naturally at $\phi = 0$.

The sequence of solution consists of three stages, which solve separately the following parts of the problem: (i) the fluid state, by solving the Navier–Stokes (NS) equations over the two-fluid domain; (ii) the transport of the LS function ϕ, which implies the displacement of the interface $\phi = 0$; and (iii) a reinitialisation of the ϕ-field for keeping the regularity of the LS function, which is specially important in the neighbourhood of the FS, and can be performed every certain number of time steps, according to the complexity of the flow (Battaglia, 2009). The numerical computation of each stage is made by different solvers of the PETSc-FEM libraries (PETSc-FEM, 2009), which are based on the Portable Extensible Toolkit for Scientific Computation (PETSc) libraries (Balay *et al*. 2008) and the Message Passing Interface (MPI, 2009) for parallel computing. The present results are obtained with an interface capturing approach that requires the synchronisation among the three solvers involved and the development of a reinitialisation stage.

The performance of the method is shown first, for the advection-renormalisation of the LS field over a typical 2D example, and second, for two- and three-dimensional dam-break problems, which are compared to the available experimental data (Martin and Moyce, 1952) and other numerical results.

2. Governing Equations

The Partial Differential Equation (PDE) systems presented in this section are solved by FEM, and each one is related to the each stage of the solution. The NS and the advective (ADV) solvers have been previously analysed (Sonzogni *et al*. 2002; Storti *et al*. 2008), while the so-called bounded renormalisation with continuous penalisation (BRCP) algorithm, which renormalises the LS function field, was introduced only for advection-renormalisation problems (Battaglia *et al*. in press).

The multi-physics programming paradigm for the synchronisation of the FEM modules was introduced in previous works (Battaglia *et al*. 2006). The three stages of solution run independently in parallel, and they are linked by C++ synchronisation programs named *hooks*, which are run at certain points in the FEM modules execution. The concept of the hooks has been borrowed from the GNU Emacs editor and from the Linux (2010) kernel. The hooks allow the data exchange among NS, ADV and BRCP solvers through the use of queues (first-in-first-out, FIFO). In each time step, the fluid velocities determined by the NS solver are sent to the ADV one for performing the LS function advection. Then, the LS field is sent to the BRCP module, where the renormalisation is performed. After that, the NS stage receives the LS field, which is needed to determine the fluid properties in the whole domain for the following time step.

The time dependence is present in two of the three stages, the NS and the ADV, for which time integration is performed by the trapezoidal rule with parameter α, with $\alpha = 1$ for the backward Euler method and $\alpha = 0.5$ for Crank–Nicolson.

2.1. Fluid state

The fluid state in the domain Ω for time $t \in [0,T]$ is given by the NS equations system for two incompressible and immiscible fluids, which is:

$$\begin{aligned} \rho(\phi(\mathbf{x},t))(\partial_t \mathbf{v} + \mathbf{v}\cdot\nabla\mathbf{v} - \mathbf{f}) - \nabla\cdot\sigma = 0; \\ \nabla\cdot\mathbf{v} = 0; \end{aligned} \tag{1}$$

where $\mathbf{x} \in \Omega$ is the position vector, $\mathbf{v}$ is the fluid velocity, $\mathbf{f}$ is the body force by unit of mass, $\rho(\phi(\mathbf{x},t))$ is the fluid density, $\partial_t(\ldots) = \partial(\ldots)/\partial t$ indicates the partial time derivative and ϕ is the LS function.

The fluid stress tensor $\boldsymbol{\sigma}$ is decomposed in an isotropic $-p\mathbf{I}$ part and a deviatoric one $\mathbf{T}$,

$$\boldsymbol{\sigma} = -p\mathbf{I} + \mathbf{T}; \tag{2}$$

where p is the pressure, $\mathbf{I}$ the identity tensor and $\mathbf{T}$ the viscous forces tensor,

$$\mathbf{T} = 2\,\mu(\phi(\mathbf{x},t))\boldsymbol{\varepsilon}; \tag{3}$$

which is a function of the strain rate tensor $\boldsymbol{\varepsilon}$ determined as

$$\boldsymbol{\varepsilon} = \frac{1}{2}[\nabla\mathbf{v} + (\nabla\mathbf{v})^T]; \tag{4}$$

for Newtonian fluids, with $(\ldots)^T$ indicating transposition and $\mu = \mu(\phi(\mathbf{x},t))$ the dynamic viscosity.

The fluid properties, density and viscosity, depend on both, the position $\mathbf{x}$ and the evaluation time t due to the multiphase model, which is given by the LS function ϕ, defined over the whole domain Ω.

The values taken by ϕ indicate whether the region Ω is occupied by one or another fluid (Sussman and Smereka, 1997), according to the following,

$$\phi(\mathbf{x},t)\begin{cases} >0 & \text{if} \quad \mathbf{x}\in\Omega_l; \\ =0 & \text{if} \quad \mathbf{x}\in\Gamma_{\mathrm{FS}}; \\ <0 & \text{if} \quad \mathbf{x}\in\Omega_g; \end{cases} \tag{5}$$

where the subdomain Ω_{l} corresponds to the liquid phase and Ω_{g} is the gaseous one, while both conditions $\Omega=\Omega_{\mathrm{l}}\cup\Omega_{\mathrm{g}}$ and $\Omega_{\mathrm{l}}\cap\Omega_{\mathrm{g}}=\phi$ are verified. Note that the subindex adopted, l and g, correspond to the liquid and the gaseous regions, respectively. Particularly, the FS is defined as

$$\Gamma_{\mathrm{FS}}=\{\mathbf{x}|\phi(\mathbf{x},t)=0\}. \tag{6}$$

In this case, due to the renormalisation method proposed for the LS function ϕ, see section 2.3, the function is bounded, i.e. $-1\le\phi\le 1$, and the transition between fluids is smooth.

Given the LS value ϕ, the fluid properties for Equations (1) and (4) are given as

$$\begin{aligned} \rho(\phi)&=\frac{1}{2}\left[\left(1+\tilde{H}(\phi)\right)\rho_l+\left(1-\tilde{H}(\phi)\right)\rho_g\right]; \\ \mu(\phi)&=\frac{1}{2}\left[\left(1+\tilde{H}(\phi)\right)\mu_l+\left(1-\tilde{H}(\phi)\right)\mu_g\right]; \end{aligned} \tag{7}$$

where the smeared Heaviside function $\tilde{H}(\phi)$ is determined through:

$$\tilde{H}(\phi)=\tanh\left(\frac{\pi\phi}{\tilde{\varepsilon}}\right); \tag{8}$$

where $\tilde{\varepsilon}$ is a reference parameter for the transition width. In this case, for $|\phi|\to\tilde{\varepsilon},\tilde{H}(\phi)\to 1$, with the consequence of a diminishing in the width of the transition for the fluid properties needed for the NS system in comparison to the transition between $\phi=-1$ and $\phi=1$ considered in the ADV step. In particular, $\tilde{\varepsilon}=0.5$ is adopted, reducing the transition length in about 70%.

The infinitely differentiable function $\tilde{H}(\phi)$ given in Equation (8) is slightly different from the other smooth Heaviside-like functions found in the literature (Sussman and Smereka 1997; Olsson and Kreiss 2005; Kurioka and Dowling 2009) because it counts on a simpler mathematical expression, and it is not piecewise defined. This condition constitutes an advantage, because the selected function naturally fits the bounds $|\phi|\le 1$ required by Equation (7) for the interpolation of the fluid properties.

For the fluid flow problems considered in this work, slip boundary conditions for the velocity $\mathbf{v}$ in Equation (1) are given over the solid boundaries Γ_{wall}, while in the case of the pressure, $p=0$ is imposed on top of the domain.

The solution of Equation (1) is made through the NS solver from the PETSc-FEM libraries (Sonzogni *et al.* 2002), adopting linear elements with the same interpolation for velocity and pressure fields, which are stabilised with streamline upwind/Petrov-Galerkin (SUPG) (Brooks and Hughes, 1982) and pressure stabilising/Petrov-Galerkin (PSPG) (Tezduyar *et al.* 1992).

2.2. Level set function advection

The transport of the LS function ϕ over the domain Ω is produced by the velocity $\mathbf{v}$ obtained by solving the NS equations, as follows,

$$\partial_t\phi+\mathbf{v}\cdot\nabla\phi=0; \tag{9}$$

with boundary conditions given by

$$\phi=\bar{\phi} \quad \text{over} \quad \Gamma_{\mathrm{in}}; \tag{10}$$

where the inflow section is $\Gamma_{\mathrm{in}}=\{\Gamma|\mathbf{v}\cdot\mathbf{n}<0\}$. In this way, the advection procedure takes into account the transport of the interface Γ_{FS} in a natural way.

This transport step, named ADV, is numerically solved by the advective module of the PETSc-FEM program (Storti *et al.* 2008). The numerical instabilities, which arise from the use of a Galerkin central scheme for solving the transport equation of the LS function ϕ, can be avoided by an SUPG strategy (Brooks and Hughes, 1982). Nevertheless, if the BRCP is performed, the SUPG stabilisation is not necessary for the transport of the LS function.

2.3. Reinitialisation of the level set function field

Most LS approximations include a renormalisation step, where a distance function equation is solved with the aim of keeping the regularity and the smoothness of the ϕ-field; otherwise, the advection of ϕ or the interpolation of the fluid properties across the interface would lose precision in the numerical solution. Since some redistancing procedures are extremely expensive (Hysing 2007), they are gradually replaced by improved algorithms (Mut *et al.* 2006, Elias *et al.* 2007). An alternative to the redistancing strategy consists of avoiding any reinitialisation by performing a highly accurate transport of the LS field, such as discontinuous Galerkin methods (Marchandise and Remacle, 2006), high-order weighted essentially non-oscillatory method, WENO (Kurioka and Dowling, 2009), or mesh adaptivity near $\phi=0$ (Marchandise and Remacle, 2006), among others.

In this work, the renormalisation process is focused on conserving the regularity of the transition between phases by solving a PDE, introduced by Battaglia (2009).

A similar strategy is the Conservative Level Set method (Olsson and Kreiss 2005; Olsson *et al.* 2007), although it does not count on a penalisation term as in the present work.

The reinitialisation consists of solving the PDE system by FEM, where the variable is ϕ. The operator BRCP is

$$\phi\,(\phi^2 - \phi_{\text{ref}}^2) - \kappa\Delta\phi + M\big(\hat{H}(\phi) - \hat{H}(\phi^0)\big) = 0; \quad (11)$$

where κ is a diffusive parameter, M a penalty coefficient and ϕ_{ref} a reference value for the variable ϕ, adopted as $\phi_{\text{ref}} = 1$, while ϕ^0 is the initial LS function value for the renormalisation step provided by the solution of Equation (9). The diffusion parameter κ, with squared length units, is related to an adopted typical element size h, usually from h^2 to $(3h)^2$, depending on the FS behaviour, such that a lower κ provides a thinner transition.

The positive coefficient M is non-dimensional and should be adopted as $O\big(10^{n_d+2}\big)$, with n_{d} the number of spatial dimensions involved. Furthermore, the function adopted for the penalising term, $\hat{H}(\phi)$, has the continuous expression

$$\hat{H}(\varphi) = \tanh(2\pi\phi); \quad (12)$$

which is a smeared Heaviside function. The purpose of selecting a smooth function which is continuous across the interface is to avoid a complicated numerical treatment, especially in three-dimensional problems.

The effect of Equation (11) can be explained as follows. The first two terms constitute a steady heat conduction equation with a source term, ϕ being the temperature, i.e.

$$\kappa\Delta\phi + Q(\phi) = 0; \quad (13)$$

where $Q(\phi) = -\phi(\phi^2 - \phi_{\text{ref}}^2)$ is the source term and κ acts as a thermal diffusivity parameter.

Physically, the source term $Q(\phi)$ forces ϕ to reach the *stable equilibrium temperatures*, i.e. those ϕ^* for which $Q(\phi^*) = 0$ and $Q'(\phi^*) < 0$, with $Q'(\phi) = \mathrm{d}Q/\mathrm{d}\phi$. Since $Q(\phi^*) = 0$, a spatially constant solution $\phi = \phi^*$ is a solution of Equation (13). Therefore, if $\phi = \phi^* + \delta\phi$, with $\delta\phi$ a small perturbation, the source term is negative due to the condition $Q'(\phi^*) < 0$, and ϕ tends to ϕ^*, independently of the sign of $\delta\phi$. For the renormalisation method, this condition is analogous for the roots $\phi^* = \pm\phi_{\text{ref}}$. Conversely, when $Q(\phi^{**}) = 0$ and $Q'(\phi^{**}) > 0$, the roots ϕ^{**} are *unstable equilibrium temperatures*, and any perturbation $\delta\phi$ produces a positive increment in the source term, taking ϕ away from the equilibrium value ϕ^{**}, as occurs when $\phi = 0$ in Equation (13).

Furthermore, the Laplacian term in Equation (13) produces a smooth transition of semiwidth $\delta = \mathcal{O}(\kappa^{1/2})$ between the bounds given by the stable roots of the source term, which are $\phi^* = \pm\phi_{\text{ref}}$. Therefore, it is verified that a larger value of the diffusivity leads to a wider transition. This is shown in Figure 1 for a steady problem with initial conditions given by piecewise-constants values for ϕ^0, and the solutions of Equation (13) corresponding to different values of diffusivity.

When Equation (11) is numerically solved over an unstructured or locally refined mesh, the diffusivity κ should be chosen considering a given δ value, i.e. $\kappa = \mathcal{O}(\delta^2)$. An appropriate transition semiwidth δ can be given by the size of two or three elements near the interface $\phi = 0$, regarding the precision of the numerical advection step.

The last term of Equation (11), or penalising term, takes into account the known values ϕ^0, i.e. those determined in the advection step. The aim of this term is to avoid the displacement of $\phi = 0$, i.e. the mass loss during the renormalisation process, by weighting $\hat{H}(\phi) - \hat{H}(\phi^0)$. Convenient values for the penalty M are $\mathcal{O}(10^{n_{\text{d}}+2})$, while low values such as $M = 1$, lead to a higher error in the interface position, and with $M = 0$ the algorithm fails because it lacks the reference ϕ^0 from the advective step. For $M > \mathcal{O}(10^{n_{\text{d}}+2})$, the renormalisation effect is lost, because the ϕ-field tends to the ϕ^0 -field, and the solution given by the ADV step is recovered (Battaglia *et al.* (in press)). Penalty parameters for preserving the interface position were also proposed by other authors, as in the Edge-Tracked Interface Locator Technique (ETILT) method (Tezduyar 2006; Cruchaga *et al.* 2007).

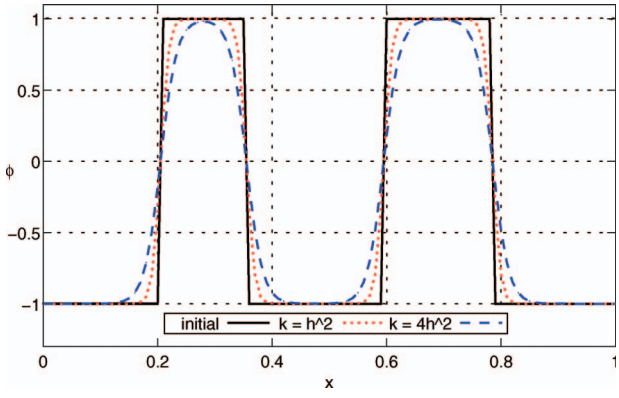

Figure 1. Artificial reaction–diffusion problem for renormalisation of ϕ depending on the diffusion coefficient κ value.

The renormalisation process acts mainly in the neighbourhood of the FS, where the loss of precision in the FS position and the mass loss are registered (Mut *et al.* 2006; Cruchaga *et al.* 2007). On the other hand, when $\phi \approx \phi_{\text{ref}}$, i.e. far from the interface, the three terms in Equation (11) tend to zero. Finally, the operator of Equation (11) is numerically solved by FEM on each time step or every n_{reno} time steps, after the computation of the ADV stage.

3. Numerical examples

3.1. *Advection-renormalisation problem: the disk of Zalesak*

The effectiveness of the renormalisation method is evaluated by solving the problem presented by Zalesak (1979) and reproduced by several authors (Mut *et al.* 2006, Elias and Coutinho 2007, Gois *et al.* 2008), which consists of a notched disk inside a square unit domain with $0 \leq (x, y) \leq 1$. The initial conditions are shown in Figure 2, being the radius $R_d = 0.15$ m, while the notch $w_d = 0.05$ m wide and $h_d = 0.25$ m height. The disk is centred at $(x_d, y_d) = (0.5,0.75)$ m at the beginning of the computation, Figure 3, enclosing the $\phi > 0$ region, and the velocity field is given by

$$\begin{aligned} v_x &= 2\pi(y - y_c); \\ v_y &= -2\pi(x - x_c); \end{aligned} \tag{14}$$

which produces a rigid rotation of the notched disk around the point $(x_c, y_c) = (0.5,0.5)$ m. After one revolution, the numerical results are compared to the initial position, that should be recovered.

The problem is solved by two different strategies: using only Equation (9), and with Equation (9) plus the periodic renormalisation with Equation (11), named ADV and ADV + BRCP, respectively. For one revolution, the final time of $t_f = 1$ s is discretised in 628 time steps of $\Delta t = 1/(200\pi)$ s ≈ 0.0016 s, with an implicit time integration considering $\alpha = 0.7$ for the trapezoidal rule. The finite element mesh consists of 128^2 bilinear quadrilateral elements of typical size $h = 7.8 \times 10^{-3}$ m.

The diffusivities for the renormalised examples are $\kappa_A = 2h^2 = 1.22 \times 10^{-4}$ m^2 in case ADV + BRCP(A), or $\kappa_B = 4h^2 = 2.44 \times 10^{-4}$ m^2 in case ADV + BRCP(B), while the penalty is chosen as $M = 10{,}000$ in both cases. The renormalisation is performed every $n_{\text{reno}} = 4$ advection time steps.

The performance of the three solution alternatives are shown in Figure 4, where the profiles of $\phi = 0$ in $t = 1$ s are represented for the three alternatives: (a) pure advection, (b) advection plus renormalisation with $\kappa_A = 2h^2$ and (c) advection plus renormalisation with $\kappa_B = 4h^2$. Note that in the pure advection case the notch is almost disappeared, while in (b) it is well captured. Furthermore, the disappearance of the notch in (c) is attributed to the wider transition induced by a higher value of κ than in (b), as explained in section 2.3. The shape distortion of the disk in the results computed with ADV + BRCP(A) is similar to the one presented by Kurioka and Dowling (2009) for the same problem with a 100^2 elements mesh and a high-order advection solver.

Regarding area conservation of the $\phi > 0$ region, there are few differences among the alternatives ADV and ADV + BRCP(B), where the disk gains between 9 and 10% of area due to the disappearance of the notch, while in case ADV + BRCP(A) the area decreases about 1%.

Figure 5 shows the LS function field for (a) ADV and (b) ADV + BRCP(A). In the first case, the transition from -1 to $+1$ is not uniform, the relief is smoothed, and the notched disk tends to disappear. In case ADV + BRCP, the transition presents uniform width around the whole $\phi = 0$ curve. Then, the constant width provided by the BRCP stage replaces the redistancing procedures classically performed in LS

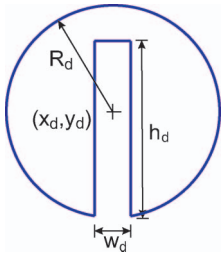

Figure 2. Shape of $\phi = 0$ for the disk of the Zalesak test.

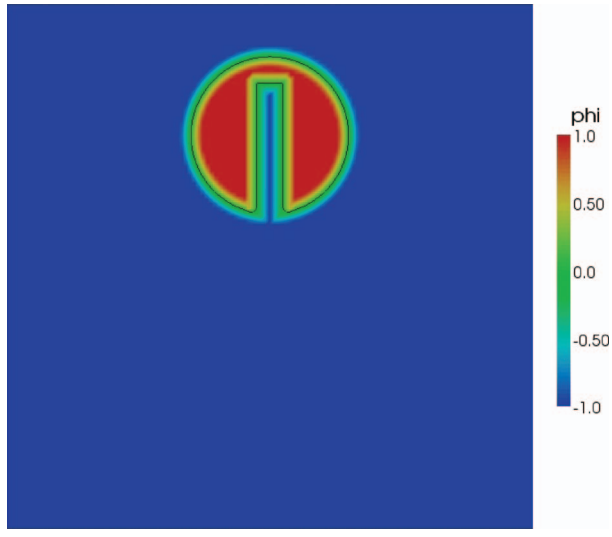

Figure 3. Initial level set function field for the notched disk for $h = 7.8 \times 10^{-3}$ m.

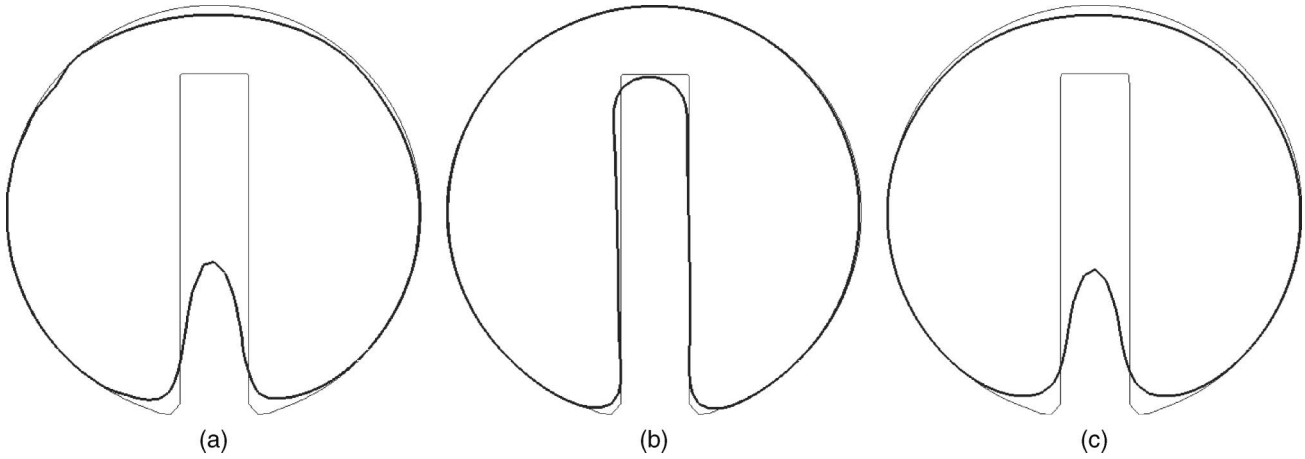

Figure 4. Curve of $\phi = 0$ for the disk of Zalesak at $t = 1$ s solved without and with BRCP (thick lines), together with the initial condition (thin lines); (a) ADV; (b) ADV + BRCP (A); (c) ADV + BRCP (B).

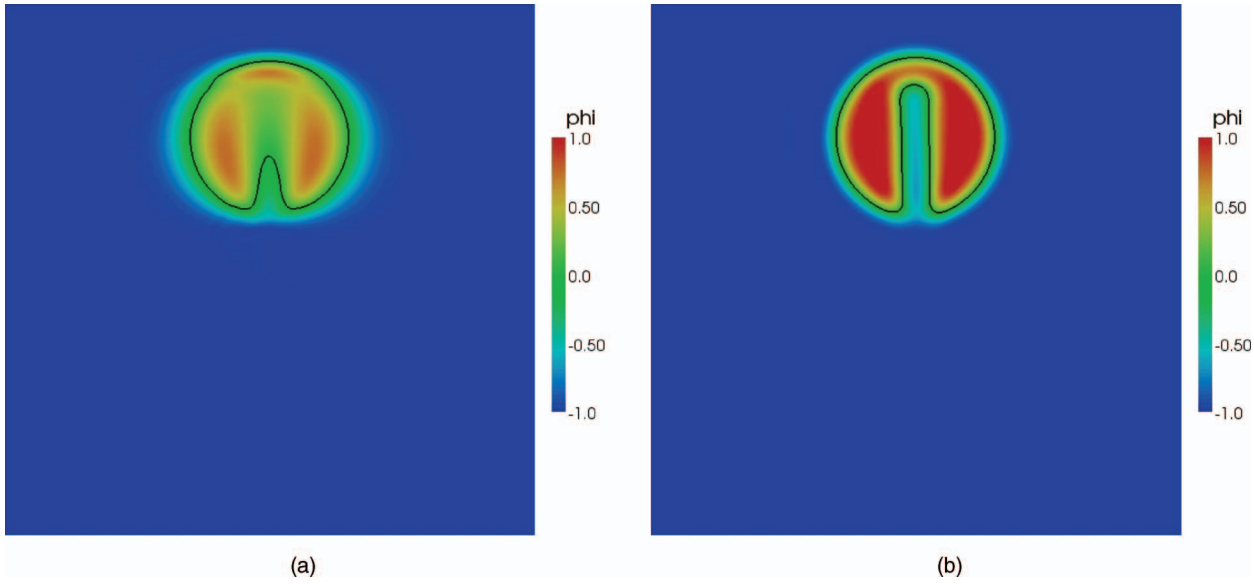

Figure 5. Level set function field at $t = 1$ s for the case of the notched disk; (a) ADV; (b) ADV + BRCP(A).

methods (Sussman and Smereka, 1997; Sussman *et al.* 1999).

Additionally, the same problem is solved with ADV + BRCP over a 256^2 elements mesh with time step $\Delta t_r = 8 \times 10^{-4}$ s, diffusivity $\kappa_r = 2h_r^2 = 3.05 \times 10^{-5}$ m^2, penalty $M_r = 10{,}000$ and $n_{reno} = 4$. The LS function field and the final profile obtained with this refined mesh are shown in Figure 6.

The difference in the width of the transitions in Figures 6(a) and 5(b) is due to the diffusivity values chosen in each case, which are $\kappa_r = 3.05 \times 10^{-5}$ m^2 and $\kappa_A = 1.22 \times 10^{-4}$ m^2, respectively. Regarding the property $\delta = \mathcal{O}(\kappa^{1/2})$, then $\delta_r \approx 2\kappa_r^{1/2} = 0.012$ m for Figure 6(a) and $\delta_A \approx 2\kappa_A^{1/2} = 0.022$ m for Figure 5(b). Furthermore, for the case ADV + BRCP(B), $\kappa_B = 2.44 \times 10^{-4}$ m^2 and $\delta_B \approx 2\kappa_B^{1/2} = 0.032$ m $> w_d/2$, i.e. the proposed transition is too smooth and the method is not able to keep the notch width, as shown in Figure 4(c).

3.2. *Collapse of a liquid column in 2D*

This example is a typical test for interface-capturing methods (Marchandise and Remacle 2006, Cruchaga *et al.* 2007, Elias and Coutinho 2007, Tang *et al.* 2008, Kurioka and Dowling 2009), consisting of a two-dimensional water column which collapses after being liberated, and is also known as the *dam-break problem*.

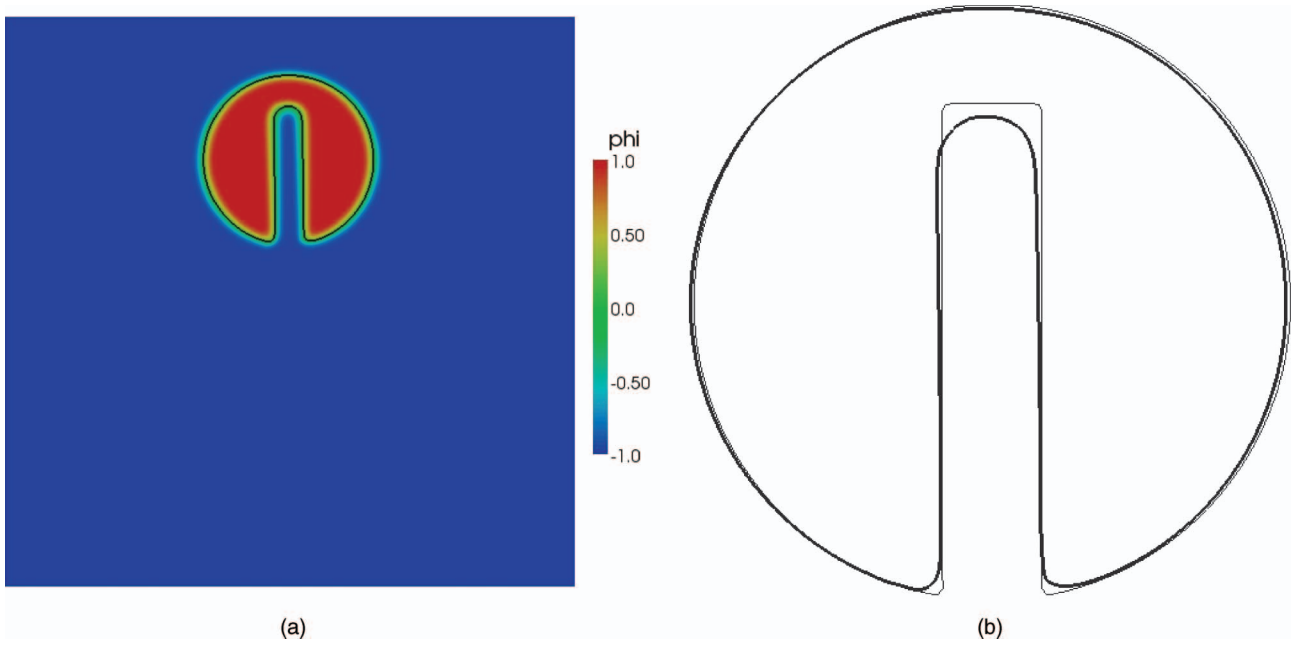

Figure 6. Results of the analysis for the rotating disk with the refined mesh; (a) LS function field; (b) initial (thin) and final (thick) $\phi = 0$ profiles.

Experimental results are available for different geometrical configurations and fluids, e.g. see Martin and Moyce (1952), Cruchaga *et al.* (2007), allowing the validation of numerical methods.

The domain Ω considered for the numerical simulation is illustrated in Figure 7, being the domain of width and height $W_d = 0.228$ m and $H_d = 0.228$ m, respectively, while the initial liquid domain Ω_l – the water column – is $W_c = 0.057$ m width and $H_c = 0.114$ m height, resulting in an aspect ratio of $r_a = H_c/W_c = 2$, the same as in the physical model of Martin and Moyce (1952).

The fluids considered for the simulation are air for the gaseous phase, with density $\rho_g = 1$ kg/m^3 and dynamic viscosity $\mu_g = 1.0 \times 10^{-5}$ kg/(m s), and water for the liquid phase, with its density and dynamic viscosity being $\rho_l = 1{,}000$ kg/m^3 and $\mu_l = 1.0 \times 10^{-3}$ kg/(m s), respectively.

For the fluid problem, boundary conditions are a perfect slip over the whole contour, $\mathbf{v} \cdot \mathbf{n} = 0$, as indicated in Figure 7, where $\mathbf{n}$ is the unit normal to the contour, and null pressure on the top of the domain. Boundary conditions for the transport problem are not required because there are no inflow sections for the domain Ω.

The initial velocity field is $\mathbf{v}_0 = \mathbf{0}$ for the NS and the ADV problems, while the initial LS function field is given such that the water column Ω_l includes nodes where $0 < \phi \leq 1$, while in the rest of the domain Ω, i.e. the gaseous phase Ω_g, is $-1 \leq \phi < 0$, and $\phi = 0$ is the initial FS position. For the numerical simulation,

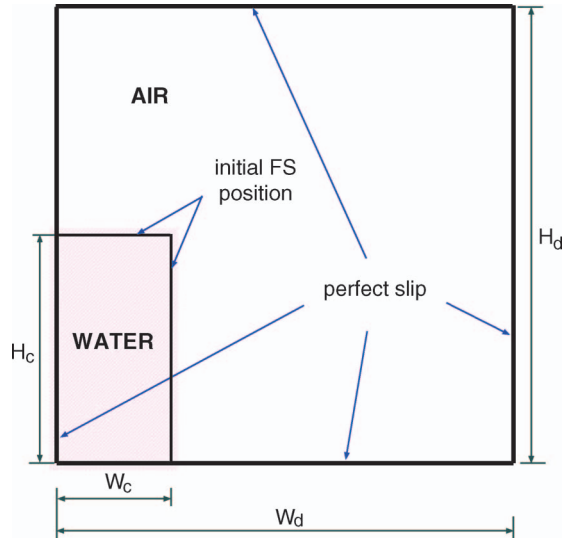

Figure 7. Geometry and boundary conditions for the collapse of a water column example in 2D.

the gate is instantaneously removed and the column collapses due to the gravity acceleration $g = 9.81$ m/s^2.

The numerical problem is solved for a uniform structured finite element mesh composed by quadrilaterals with typical size $h \approx 0.0023$ m and approximately 10,200 nodes, which is the same for the three stages to be solved: NS, ADV and BRCP. The time step adopted is $\Delta t = 0.002$ s along 1,000 time steps, with an implicit temporal integration for the NS and

the ADV problems, considering an integration parameter $\alpha = 0.7$ for the trapezoidal rule, while the BRCP stage is stationary each time step.

The reinitialisation step is proposed with parameters $\kappa = 2h^2 = 1.04 \times 10^{-5}$ m^2 and $M = 10{,}000$. The number of ADV steps which are performed before each reinitialisation is $n_{\text{reno}} = 2$ for this particular example.

In Figure 8, The dimensionless front position $x_f(t^*)/W_c$ is represented versus the dimensionless time $t^* = t\sqrt{2g/W_c}$, for the numerical results and the experimental measurements taken from Martin and Moyce (1952). In that figure, the slope of the curve represents the velocity of the advancing front, which is well captured.

Other reference results, also represented in Figure 8, were numerically obtained by using the ETILT method, from Cruchaga *et al.* (2007), and a VOF approach developed by Elias and Coutinho (2007). In both references, the aspect ratio is $r_a = H_c/W_c = 2$, which means that there is a physical similarity of the problem solved with different W_c values, according to the dimensionless front position and dimensionless time. Furthermore, Elias and Coutinho (2007) solved the collapse of the column in a 3D domain instead a two-dimensional one.

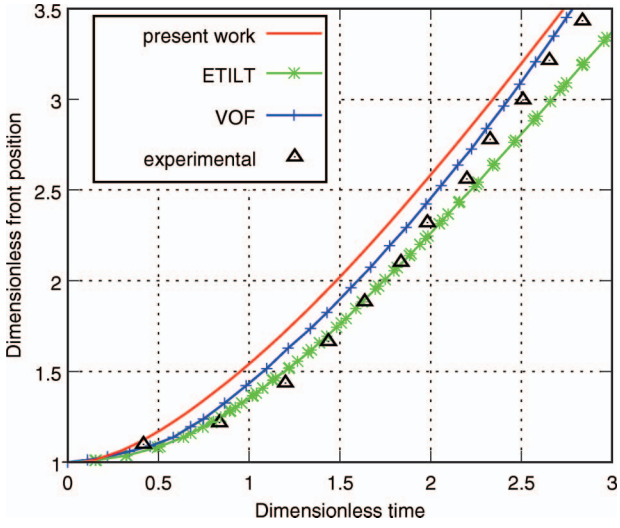

Figure 8. Dimensionless front position $x_f(t^*)/W_c$ versus dimensionless time $t^* = t\sqrt{2g/W_c}$ for the 2D dam-break problem: numerical results and experimental data.

The evolution of the dimensionless water height $h_c(t^*)/W_c$, measured over the left side of the domain, is represented as a function of the dimensionless time $t^* = t\sqrt{2g/W_c}$ in Figure 9. In that figure, the displacement of the numerical curve from the experimental one is smaller than in Figure 8, and the mean descending velocity is well captured, considering the slope of the curves. Again, numerical reference results are taken from Cruchaga *et al.* (2007) and Elias and Coutinho (2007), which are also included in Figure 9.

The FS position in different instants of the simulation are shown in Figure 10, including early stages without breaking, as in $t = 0.14$ s or $t = 0.28$ s, and later stages with air capture and interface merging.

3.3. *Collapse of a liquid column in 3D*

The three-dimensional example presented is the numerical simulation of the collapse of a cylindrical water column, which was also experimentally studied by Martin and Moyce (1952). The problem was solved for one-fourth of the column inside a cubic domain, as represented in Figure 11, with proper boundary conditions in order to keep the symmetry of the problem, as made by other authors (Akin *et al.* 2007; Cruchaga *et al.* 2010, Tang *et al.* 2008).

The domain Ω consists of a cube with an edge length $b = 0.2284$ m, in which the water column, i.e. the fluid domain Ω_f, is centred in the corner of the

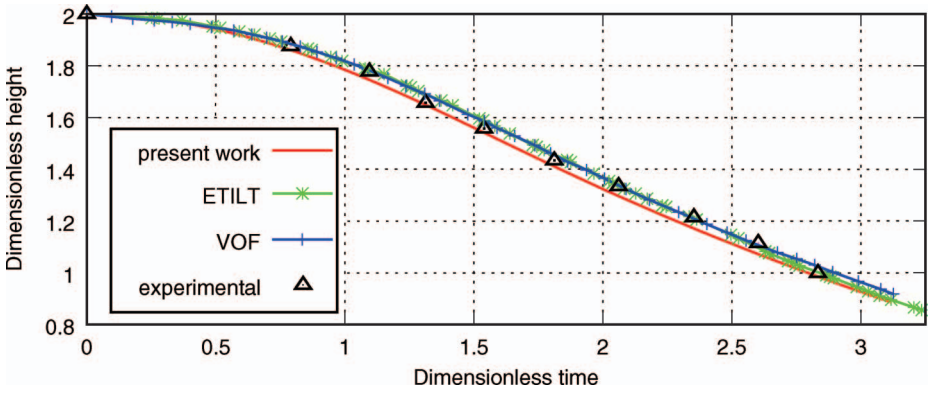

Figure 9. Dimensionless column height $h_c(t^*)/W_c$ versus dimensionless time $t^* = t\sqrt{2g/W_c}$ for the problem of the 2D dam-break problem: numerical results and experimental data.

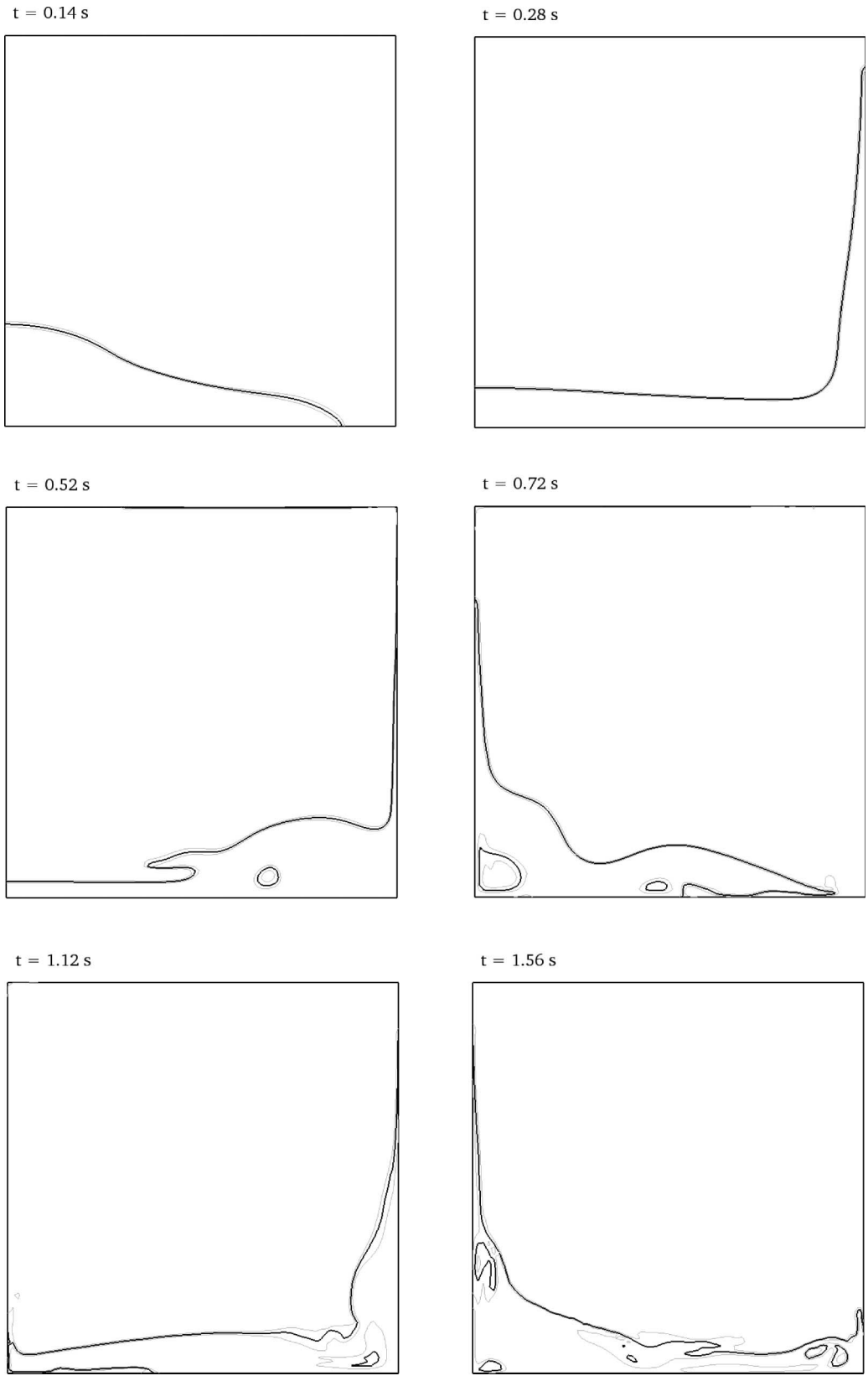

Figure 10. FS positions for several instants in the 2D dam-break problem.

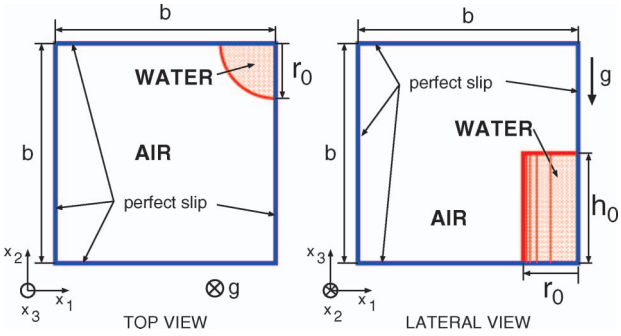

Figure 11. Geometry for the problem of the collapse of a cylindrical water column in 3D.

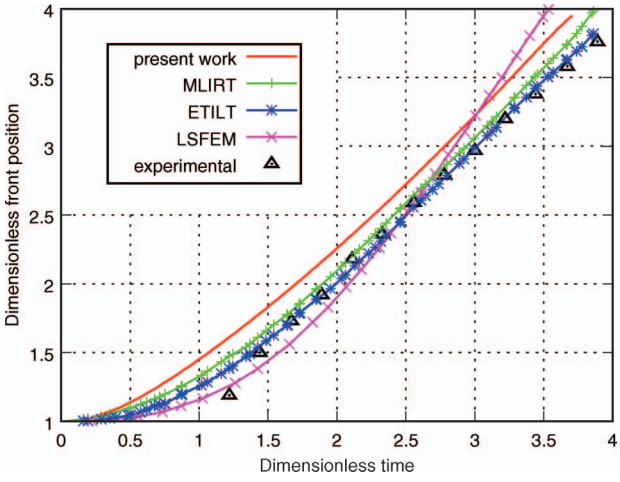

Figure 12. Dimensionless front position r_f $(t^*)/r_0$ versus dimensionless time $t^* = t\sqrt{2g/r_0}$ for the problem of the collapse of a cylindrical water column in 3D: numerical results and experimental data.

plane coordinates $(x_1,x_2) = (0.2284,0.2284)$ m, its radius and height being $r_0 = 0.0571$ m and $h_0 = 0.1142$ m, respectively, giving an aspect ratio $r_a = 2$, see Figure 11.

The collapse is started once the column is released instantaneously at time $t = 0$ due to the action of the gravity acceleration $g = 9.81\text{m/s}^2$, given in $-x_3$ direction. The fluid properties for water are density $\rho_l = 1{,}000$ kg/m^3 and dynamic viscosity $\mu_l = 1.0 \times 10^{-3}$ kg/(ms), while for the air are $\rho_g = 1$ kg/m^3 and $\mu_g = 1.0 \times 10^{-5}$ kg/(ms), respectively.

The finite element mesh employed for the numerical simulation counts on 50^3 hexahedral elements with uniform edge length $h \approx 4.5 \times 10^{-3}$ m. Numerical simulation is performed along 1,000 time steps of $\Delta t = 0.001$ s with implicit integration for NS and ADV, and renormalisation at each time step, i.e. $n_{\text{reno}} = 1$, adopting a penalising parameter of $M = 500{,}000$ and a diffusion coefficient $\kappa = 2h^2 = 4.17 \times 10^{-5}$ m^2. Perfect slip conditions over the walls are imposed for the NS stage, while ADV do not require boundary conditions, as in the former case.

The dimensionless front displacement $r_f(t^*)/r_0$ of the breaking column as a function of the dimensionless time $t^* = t\sqrt{2g/r_0}$ is represented in Figure 12, where the experimental measurements of Martin and Moyce (1952) are compared with the numerical results obtained through: (i) the present NS + ADV + BRCP approach, (ii) Edge-Tracked Interface Locator Technique (ETILT) and Moving Lagrangian Interface Remeshing Technique (MLIRT), both from Cruchaga *et al.* (in press), and a Least Square Finite Element Method (LSFEM) (Tang *et al.*, 2008).

Since there are no experimental results for the dimensionless height of the top of the column, only numerical results are shown in Figure 13,

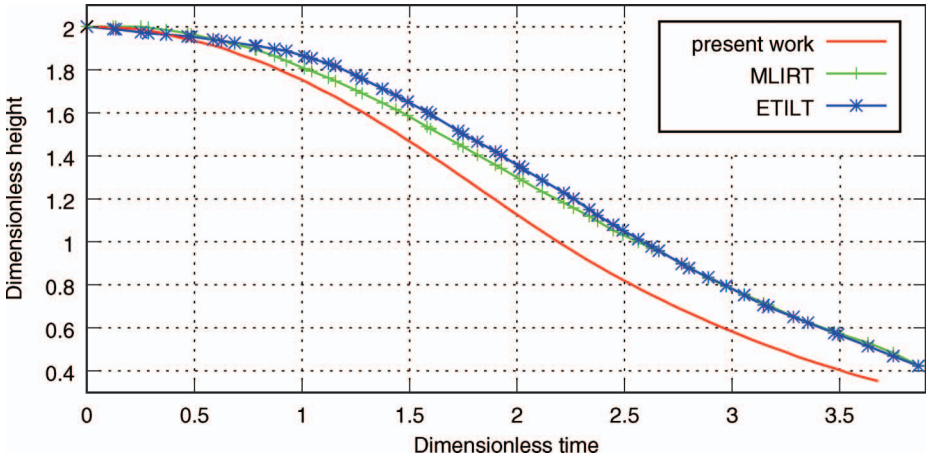

Figure 13. Dimensionless column height h_c $(t^*)/r_0$ versus dimensionless time $t^* = t\sqrt{2g/r_0}$ for the problem of the collapse of a cylindrical water column in 3D: numerical results.

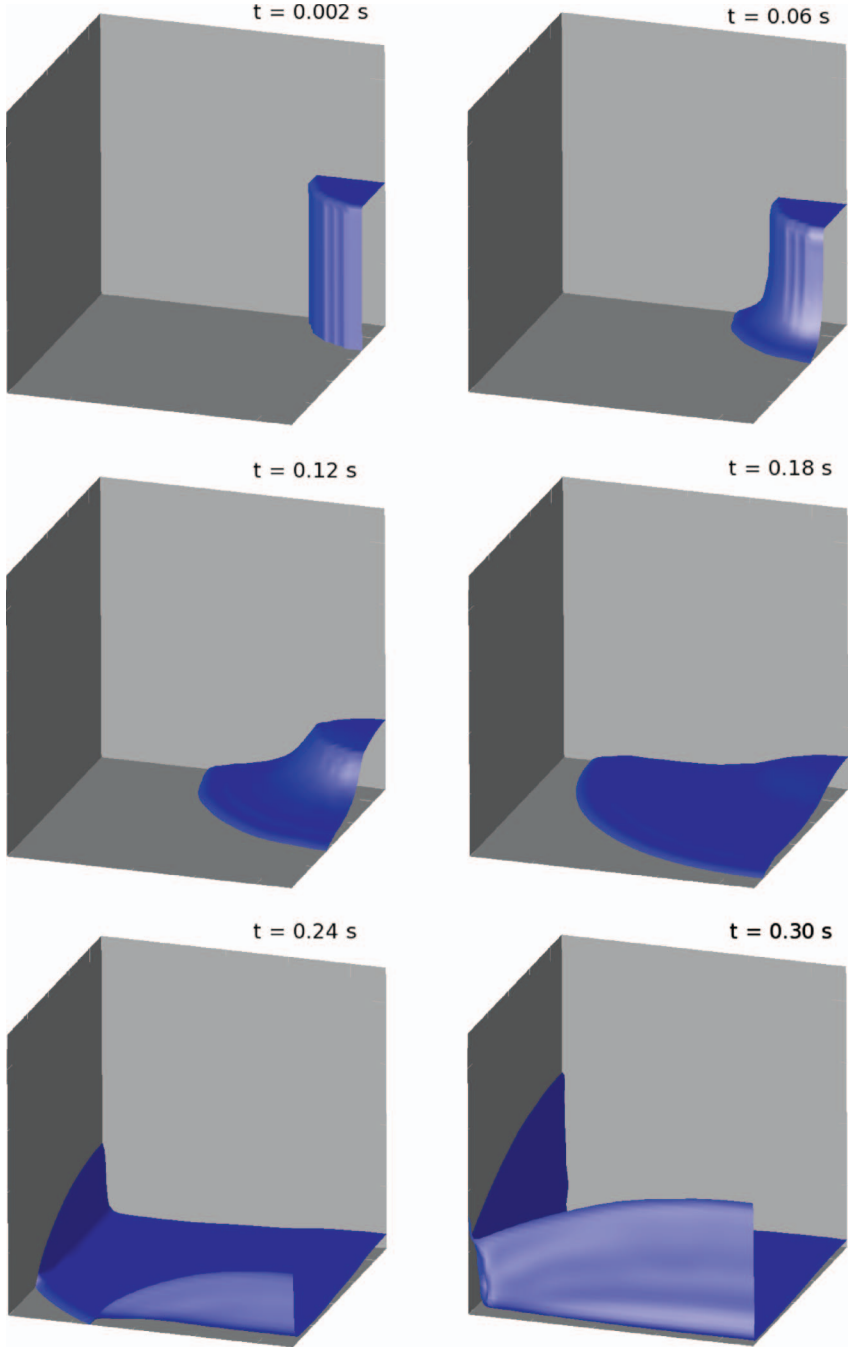

Figure 14. Initial stages for the problem of the collapse of a cylindrical water column in 3D.

corresponding to the method introduced in the present work and the results presented in Cruchaga *et al*. (2009) for ETILT and MLIRT, considering the dimensionless column height $h_c(t^*)/r_0$ as a function of the dimensionless time t^*. All these results correspond to an aspect ratio of $r_a = H_c/W_c = 2$, and then to similarity flows. The early stages of the collapse of the column are represented in Figure 14.

4. Conclusions

The simulation of viscous and incompressible FS flows is numerically performed by a three-stage FEM based on the level set approximation, consisting of: an NS solver for the fluid flow, a transport equation for the advection of the level set function field, and a renormalisation step for keeping some properties of the scalar field, in a weak-coupling paradigm. Each of

the three steps is numerically computed over the same fixed finite element mesh, and can be solved through parallel computing. Particularly, the application of a continuous operator, named BRCP, is introduced for two-fluid flow problems.

Appropriate values for the user-defined parameters required by the BRCP are directly proposed as (i) a function of the number of spatial dimensions for the penalising parameter M, and (ii) a diffusivity κ proportional to the square of the transition semiwidth between the limiting bounds of the level set function ϕ. In the latter case, the mesh size near the interface can be taken as a reference for proposing δ.

The advection and renormalisation stages are used to solve a classical test, the disk of Zalesak in section 3.1, which shows the performance of the renormalisation method for keeping the sharpness of the interface and the regularity of the level set function field obtained. The renormalisation parameters are applied according to the guidelines given in section 2.3, and the influence of the diffusivity κ over the transition width δ is verified.

Two typical two- and three-dimensional transient FS problems are solved by the three-stage methodology, in sections 3.2 and 3.3, respectively. The results are in good agreement with the experimental measurements and with the results obtained through other numerical methods taken from the literature for the early stages of the problem, showing the ability of the proposed strategy to consider large density and viscosity ratios. Furthermore, after the water impact over the walls, the present method reproduces complex topological changes, as the breaking up and merging of the FS. The BRCP coefficients M and κ were given directly by the estimations mentioned before.

The three-stage proposal can be applied to FS flows as well as to general two-fluid flows problems, taking into account that the boundary conditions in the interface are directly solved by the two-phase level set method.

Acknowledgements

This work has received financial support from Consejo Nacional de Investigaciones Científicas y Técnicas (CONICET, Argentina, grant PIP 5271/05), Universidad Nacional del Litoral (UNL, Argentina, grant CAI + D 2009–III-4–2) and Agencia Nacional de Promoción Científica y Tecnológica (ANPCyT, Argentina, grants PICT 01141/2007, PICT 1506/2006), and was partially performed with the *Free Software Foundation GNU-Project* resources such as GNU/Linux OS and GNU/Octave, as well as other Open Source resources such as PETSc, MPICH, OpenDX, ParaView, LATEX and JabRef.

References

Akin, J.E., Tezduyar, T.E., and Ungor, M., 2007. Computation of flow problems with the mixed interface-tracking/interface-capturing technique (MITICT). *Computers & Fluids*, 36 (1), 2–11.

Balay, S., *et al*., 2008. *PETSc users manual*. ANL 95/11 – Revision 3.0.0, Argonne National Laboratory.

Battaglia, L., *et al*., 2006. Numerical simulation of transient free-surface flows using a moving mesh technique. *ASME Journal of Applied Mechanics*, 73 (6), 1017–1025.

Battaglia, L., Storti, M.A., and D'Elía, J., 2007. Stabilized free-surface flows. *In*: S. Elaskar, E. Pilotta, and G. Torres, eds. *Mecánica computacional*. Vol. XXVI, 2–5, October. Cordoba, 1013–1030. Asociación Argentina de Mecánica Computacional. Available from: URL http://www.cimec.org.ar/ojs [Accessed 23 October 2009].

Battaglia, L., Storti, M.A., and D'Elía, J., in press. Bounded renormalization with continuous penalization for level set interface capturing methods. *International Journal for Numerical Methods in Engineering*. DOI: 10.1002/nme.2925?

Battaglia, L., 2009. *Stabilized finite elements for free-surface flows: tracking and capturing of interface*. Thesis (PhD). Facultad de Ingeniería y Ciencias Hídricas, Universidad Nacional del Litoral. In Spanish.

Brooks, A. and Hughes, T.J.R., 1982. Streamline upwind/Petrov-Galerkin formulations for convection dominated flows with particular emphasis on the incompressible Navier–Stokes equations. *Computer Methods in Applied Mechanics Engineering*, 32 (1–3), 199–259.

Chippada, S., *et al*., 1996. Numerical simulation of free-boundary problems. *International Journal of Computational Fluid Dynamics*, 7 (1), 91–118.

Cruchaga, M., *et al*., 2010. A surface remeshing technique for a Lagrangian description of 3D two-fluid flow problems. *International Journal for Numerical Methods in Fluids*, 63 (4), 415–430.

Cruchaga, M.A., Celentano, D.J., and Tezduyar, T.E., 2007. Collapse of a liquid column: numerical simulation and experimental validation. *Computational Mechanics*, 39, 453–476.

Elias, R. and Coutinho, A.L.G.A., 2007. Stabilized edge-based finite element simulation of free-surface flows. *International Journal for Numerical Methods in Fluids*, 54 (6–8), 965–993.

Elias, R., Martins, M.A.D., and Coutinho, A.L.G.A., 2007. Simple finite element-based computation of distance functions in unstructured grids. *International Journal for Numerical Methods in Engineering*, 72 (9), 1095–1110.

Gois, J.P., *et al*., 2008. Front tracking with moving-least-squares surfaces. *Journal of Computational Physics*, 227 (22), 9643–9669.

Hirt, C.W. and Nichols, B.D., 1981. Volume of fluid (VOF) method for the dynamics of free boundaries. *Journal of Computational Physics*, 39 (1), 201–225.

Huerta, A. and Liu, W.K., 1988. Viscous flow with large free-surface motion. *Computer Methods in Applied Mechanics and Engineering*, 69, 277–324.

Hughes, T.J.R., Liu, W.K., and Zimmermann, T.K., 1981. Lagrangian-Eulerian finite element formulation for incompressible viscous flows. *Computer Methods in Applied Mechanics and Engineering*, 29 (3), 329–349.

Hysing, S.R., 2007. *Numerical simulation of immiscible fluids with FEM level set techniques*. Thesis (PhD). Dortmund, Germany.

Idelsohn, S.R., Oñate, E., and Del Pin, F., 2004. The particle finite element method: a powerful tool to solve incompressible flows with free-surfaces and breaking waves. *International Journal for Numerical Methods in Engineering*, 61 (7), 964–984.

Kurioka, S. and Dowling, D.R., 2009. Numerical simulation of free-surface flows with the level set method using an extremely high-order accuracy WENO advection scheme. *International Journal of Computational Fluid Dynamics*, 23 (3), 233–243.

Linux, 2010. *The Linux Documentation Project* [online]. Available from: http://www.gnu.org [Accessed February 2010].

Marchandise, E. and Remacle, J.F., 2006. A stabilized finite element method using a discontinuous level set approach for solving two phase incompressible flows. *Journal of Computational Physics*, 219 (2), 780–800.

Martin, J.C. and Moyce, W.J., 1952. An experimental study of the collapse of liquid columns on a rigid horizontal plane. *Philosophical Transactions of the Royal Society of London. Series A, Mathematical and Physical Sciences*, 244 (882), 312–324.

MPI, Message Passing Interface, 2009. Available from: http://www.mpi-forum.org [Accessed October 2009].

Mut, F., Buscaglia, G.C., and Dari, E.A., 2006. New mass-conserving algorithm for level set redistancing on unstructured meshes. *Journal of Applied Mechanics*, 73 (6), 1011–1016.

Olsson, E. and Kreiss, G., 2005. A conservative level set method for two phase flow. *Journal of Computational Physics*, 210 (1), 225–246.

Olsson, E., Kreiss, G., and Zahedi, S., 2007. A conservative level set method for two phase flow II. *Journal of Computational Physics*, 225 (1), 785–807.

Osher, S. and Sethian, J.A., 1988. Fronts propagating with curvature-dependent speed: algorithms based on Hamilton-Jacobi formulations. *Journal of Computational Physics*, 79 (1), 12–49.

PETSc-FEM, 2009. *A general purpose, parallel, multi-physics FEM Program* [online]. GNU General Public License (GPL). Available from: http://www.cimec.org.ar/petscfem [Accessed October 2009].

Rabier, S. and Medale, M., 2003. Computation of free-surface flows with a projection FEM in a moving mesh framework. *Computer Methods in Applied Mechanics and Engineering*, 192 (41–42), 4703–4721.

Scardovelli, R. and Zaleski, S., 1999. Direct numerical simulation of free-surface and interfacial flow. *Annual Reviews in Fluid Mechanics*, 31, 567–603.

Sethian, J.A., 1995. *A fast marching level set method for monotonically advancing fronts*. National Academy of Sciences, USA, 93, 1591–1595.

Shyy, W., *et al*., 1996. *Computational fluid dynamics with moving boundaries*. Taylor and Francis.

Sonzogni, V., *et al*., 2002. A parallel finite element program on a Beowulf Cluster. *Advances in Engineering Software*, 33, 427–443.

Storti, M.A., *et al*., 2008. Dynamic boundary conditions in computational fluid dynamics. *Computer Methods in Applied Mechanics and Engineering*, 197 (13–16), 1219–1232.

Sussman, M., *et al*., 1999. An adaptive level set approach for incompressible two-phase flows. *Journal of Computational Physics*, 148 (1), 81–124.

Sussman, M. and Smereka, P., 1997. Axisymmetric free boundary problems. *Journal of Fluid Mechanics*, 341, 269–294.

Tang, B., Li, J.F., and Wang, T.S., 2008. Viscous flow with free-surface motion by least square finite element method. *Applied Mathematics and Mechanics*, 29 (7), 943–952.

Tezduyar, T.E., 2006. Interface-tracking and interface-capturing techniques for finite element computation of moving boundaries and interfaces. *Computer Methods in Applied Mechanics and Engineering*, 195 (23–24), 2983–3000.

Tezduyar, T.E., *et al*., 1992. Incompressible flow computations with stabilized bilinear and linear-equal-order interpolation velocity-pressure elements. *Computer Methods in Applied Mechanics and Engineering*, 95 (2), 221–242.

Zalesak, S.T., 1979. Fully multidimensional flux-corrected transport algorithms for fluids. *Journal of Computational Physics*, 31 (3), 335–362.